RESEARCH ARTICLE

ADVANCED PHYSICS RESEARCH Open Access

www.advphysicsres.com

Momentum Transfer in Triboelectric Nanogenerators

Zeyang Yu, Yuyang Zhang, Morten Willatzen, Jiajia Shao, and Zhong Lin Wang**

The triboelectric nanogenerator (TENG) reflects a prospering field, that uses Maxwell's displacement current as the driving force to transform mechanical energy into electricity. Based on the law of energy conservation, many theoretical models of TENGs are proposed to provide a detailed insight into how energy flows and transformation in the energy harvesting system, while ignoring a hidden but extremely important point about TENG's momentum transfer and conservation. Here a series of analysis is presented for the momentum transfer and conservation in TENGs based on Maxwell equations and stress tensor. Using a time-dependent 3D mathematical model, it is elaborated that how the time- and spatial-dependent momentum current is influenced by the field and the dielectric materials, demonstrating that momentum is overall conserved for a TENG. In other words, the TENG device can not only convert mechanical energy into electricity, but it is also able to transfer momentum. Momentum transfer is another important characteristic of TENGs, and finally, the essential differences and similarities among the momentum transfer, energy transfer, and energy transformation in TENGs are systematically discussed. This study will certainly serve as a new starting point for exploring momentum transfer and conservation in the TENG momentum transfer system.

1. Introduction

Efficiently converting ambient chaotic mechanical energy into electricity with triboelectric nanogenerators (TENGs) has attracted vast attention and increasing interest due to its potential applications.[1,2] A series of theoretical models of TENGs such as the equivalent circuit model[3–6] and the distance-dependent electric field model[7–9] has been developed to investigate the basic working principles of TENGs. Recently, a universal time- and spatial-dependent mathematical model with varying geometric configurations in Cartesian,[10–13] cylindrical[14,15] and spherical[16] coordinate systems are presented, which can be utilized to characterize the time-varying electric field, electric polarization, electric displacement vector, and the displacement current. This is because the basic laws of electromagnetism relating various scalar and vector quantities hold irrespective of the coordinate system. On one hand, through the mathematical model it has been demonstrated that why the displacement current is the driving force of TENGs,[17–19] which allow us to clarify the energy transfer and energy transformation process of TENGs in more depth.[17,20–23] On the other hand, the established model offers a quite necessary basis for revealing the momentum transfer and conservation in TENGs, which is a fairly important question but has not hitherto received careful attention.

The momentum conservation law is one of the three fundamental conservation laws, initially a deduction of Newton's laws of motion but later discovered with much wider applicability.[24] By virtue of the homogeneity of space, the mechanical properties of a closed system are unchanged by any parallel displacement of the entire system in space. So, momentum conservation is a consequence of space translation invariance, while energy conservation law is a result of the homogeneity of time.[25,26] It is a fact that the total momentum of a system remains constant if the resultant external force is zero. A nonzero external force produces changes in the momentum of the system due to a net momentum current flowing into the system volume.[27] For a TNEG energy harvesting system, an analogy between the momentum transfer process and the energy flow process has been illustrated in **Figure 1**. And we have proved that a TENG device can not only transform mechanical energy into electricity but also transfer momentum; or a general conclusion is that momentum transfer is one of the other defining features of TENGs. In this

Z. Yu, M. Willatzen, J. Shao, Z. L. Wang
Beijing Institute of Nanoenergy and Nanosystems
Chinese Academy of Sciences
Beijing 101400, P. R. China
E-mail: shaojiajia@binn.cas.cn; zhong.wang@mse.gatech.edu
Z. Yu, M. Willatzen, J. Shao, Z. L. Wang
School of Nanoscience and Technology
University of Chinese Academy of Sciences
Beijing 100049, P. R. China
Y. Zhang
School of Material Science and Engineering
Jilin University
Changchun 130012, PR China
Y. Zhang
Department of Materials
University of Manchester
Manchester M13 9PL, UK
Z. L. Wang
School of Materials Science and Engineering
Georgia Institute of Technology
Atlanta, GA 30332-0245, USA

The ORCID identification number(s) for the author(s) of this article can be found under https://doi.org/10.1002/apxr.202300115

DOI: 10.1002/apxr.202300115

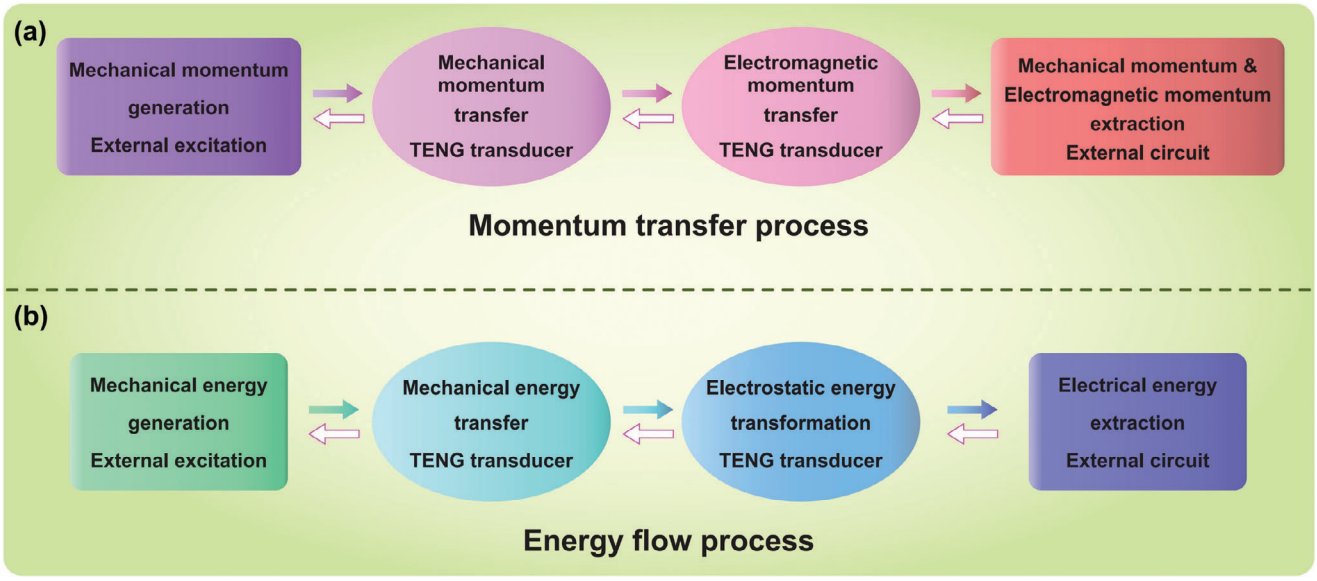

Figure 1. Schematic diagram showing an analogy between a) momentum transfer process and b) energy flow process in a momentum transfer system based on a triboelectric nanogenerator (TENG) including an external excitation, a TENG transducer, and an external circuit.

paper, the Maxwell stress tensor $\overleftrightarrow{\mathbf{T}}$ is utilized to describe the conservation of momentum within and around the TENG device, since it characterizes the dual identity of electromagnetic stress pressure and negative momentum current density.[27] It should be noticed that a periodic low-frequency motion of a TENG leads to an infinitesimally small magnetic induction $\boldsymbol{B}$, making it reasonable to neglect the magnetic induction in the expression for the energy flux density (Poynting vector $\boldsymbol{S}$) and the momentum density of electromagnetic fields.

The time-varying momentum current distribution and momentum variations within the TENG device have been systematically elucidated using Maxwell's equations and the Maxwell stress tensor. It is confirmed that momentum is conserved during the energy harvesting process. Through this method, we can obtain the specific amount of momentum absorbed and transferred by each single fraction of the TENG device at any position. Taking these into account, we may list additional constraints when optimizing the performance of TENG devices in complicated electro–mechanical coupling. Neglecting the Poynting vector, the total momentum currents absorbed by the moving part and stationary part of the TENG device, are equal in magnitude but opposite in direction. However, the transmission of momentum current is interrupted by the free charges distributed on the electrodes or the triboelectric charges in the contacting surfaces. Most importantly, this work explains how the momentum currents flowing into a Gaussian surface lead to the electromagnetic force. The total electromagnetic force acting on a volume V is equal to the momentum current passing through the closed surface S of the volume, which can also be obtained through the integration of the stress tensor over the Gaussian surface. In brief, momentum transfer is one of the important characteristics of the TENG device, and the energy harvesting system based on TENGs is also a momentum transfer system. Understanding this new discovery is a prerequisite to obtaining detailed insight into its operation and application potential.

2. General Theory

2.1. Momentum Transfer and Energy Flow Process

In Newtonian mechanics, momentum including linear momentum and angular momentum is the product of the mass and velocity of an object; while in analytical mechanics, allowing one to choose coordinate systems that incorporate symmetries and constraints, a generalized momentum is introduced.[24] Furthermore, in relativistic mechanics or in the nonrelativistic regime, the definitions of generalized momentum are also different. Though the definition of the concept varies, the principles of momentum are not substantially different. However, energy takes different forms in natural processes, and it can be converted from one form to another. According to the law of conservation of energy, energy is transferable to a different location or object, but it cannot be created or destroyed. Figure 1 illustrates an analogy diagram between the momentum transfer process and the energy flow process in TENGs. Once mechanical momentum is generated under an external excitation, it is transferred to the moving part of TENGs and then the electromagnetic momentum of fields within a TENG transducer. Finally, the external circuit obtains mechanical and electromagnetic momentum in currents. Not that the total produced momentum remains constant during the momentum transfer process. This process is similar to which energy is transferred and transformed in the energy harvesting system of external excitation, TENG transducer, and an external circuit.[3] For instance, Mechanical energy is transferred and stored in the TENG transducer in the form of electrostatic energy, and then extracted to the external circuit. Here, we put our

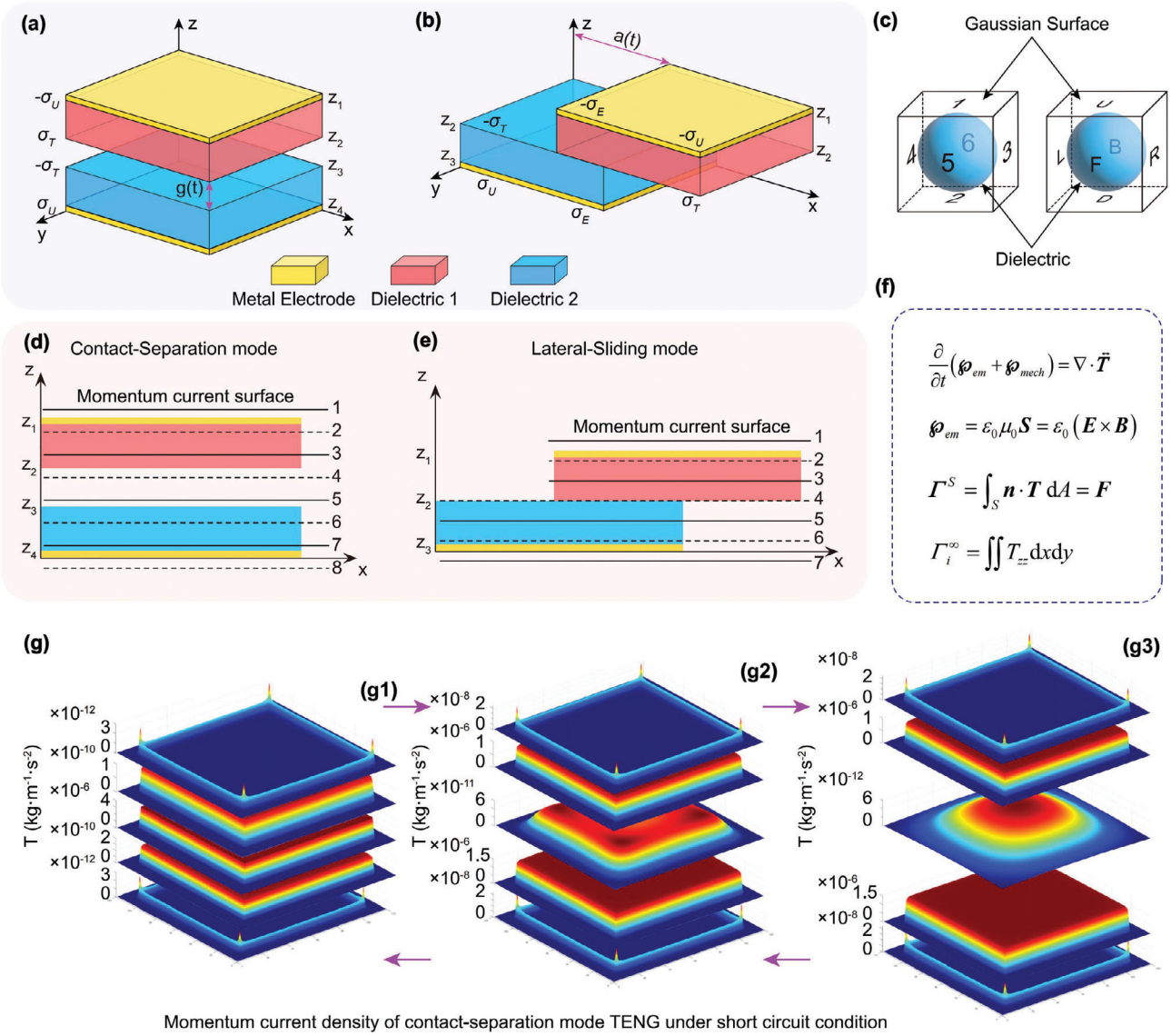

Figure 2. Schematic diagram showing 3D model of a) contact-separation mode and b) lateral-sliding mode triboelectric nanogenerator (TENG). c) Dielectric block enclosed with Gaussian surface, through which momentum current passes. Schematic diagram of d) contact-separation mode and e) lateral-sliding mode TENG, depicting infinite planes through which momentum current passes. f) Several key formulas about momentum density, momentum current and Maxwell stress tensor. g) Surface plot demonstrating momentum current density of contact-separation mode TENG under short circuit condition at the beginning (g1), quarter/three quarters (g2) and half (g3) of the cycle.

focus on the electromagnetic momentum of fields distributed in the TENG transducer, which is beneficial to understand the momentum flow in the TENG momentum transfer system. The inverted hollow arrow indicates a feed back effect of each frame to the upstream. Detailed discussions of the momentum transfer and conservation in the TENG device will be available in the subsequent parts of this work, taking the contact–separation (CS) mode and lateral sliding (LS) mode TENG as examples.

2.2. Mathematical Model of the CS and LS Mode TENG

For the CS mode TENG as presented in **Figure** 2a, assume there are two parallel square dielectric materials each attached with a metal electrode on the outside, perpendicular to the z-axis. The side length of each layer is L and the *i-th* layer possesses a uniform surface charge density σ_i at the position z_i, respectively, producing a scalar electric potential $\varphi(x, y, z)$ at an arbitrary field point $\boldsymbol{r}(x, y, z)$. As mentioned above, since the TENG is usually operated at low frequency, the generated magnetic induction is extremely weak and can be ignored. Using our proposed mathematical model,[3,10–15] the electric potential $\varphi(x, y, z)$, time-varying electric field $\boldsymbol{E}(x, y, z)$, and the relevant electric field components $[E_x(x, y, z), E_y(x, y, z), E_z(x, y, z)]$ have been obtained (see Section S1, Supporting Information). It is found by Equation (S4c, Supporting Information) that the z-component of the electric field along the symmetry axis $E_z(L/2, L/2, z)$ is[10]:

$$E_z\left(\frac{L}{2},\ \frac{L}{2},\ z\right)=\sum_{i=1}^{4}\frac{\sigma_i}{\pi\varepsilon\,(\mathbf{r})}\arctan\frac{L^2}{4\left(z-z_i\right)\sqrt{L^2/2+\left(z-z_i\right)^2}}$$
$$=-\frac{\sigma_U}{\pi\varepsilon\,(\mathbf{r})}\arctan\frac{L^2}{4\left(z-z_1\right)\sqrt{L^2/2+\left(z-z_1\right)^2}}$$
$$+\frac{\sigma_T}{\pi\varepsilon\,(\mathbf{r})}\arctan\frac{L^2}{4\left(z-z_2\right)\sqrt{L^2/2+\left(z-z_2\right)^2}}$$
$$-\frac{\sigma_T}{\pi\varepsilon\,(\mathbf{r})}\arctan\frac{L^2}{4\left(z-z_3\right)\sqrt{L^2/2+\left(z-z_3\right)^2}}$$
$$+\frac{\sigma_U}{\pi\varepsilon\,(\mathbf{r})}\arctan\frac{L^2}{4\left(z-z_4\right)\sqrt{L^2/2+\left(z-z_4\right)^2}} \tag{1}$$

where σ_T and σ_U represent the triboelectric charge density and transferred charge density in Figure 2a, respectively; and the L is the length of the electrode/dielectric. When an external resistor R is connected, the governing equation of the CS mode TENG is given by:

$$RL^2\frac{\mathrm{d}\sigma_U}{\mathrm{d}t}=\int_{z_4}^{z_1}E_z\left(\frac{L}{2},\ \frac{L}{2},\ z\right)\mathrm{d}z \tag{2}$$

Subsequently, the average power output at steady state becomes:

$$P_{av,CS}=\frac{1}{T}\int_0^T R\left(L^2\frac{d\sigma_U}{dt}\right)^2\mathrm{d}t \tag{3}$$

and one can derive the best matching resistance for CS mode TENG by optimizing the average power output.

A similar method is applied to the LS mode TENG (Figure 2b). The electric potential $\varphi(x, y, z)$, electric field $\boldsymbol{E}(x, y, z)$, and the relevant electric field components [$E_x(x, y, z)$, $E_y(x, y, z)$, $E_z(x, y, z)$] have been derived systematically (see Section S2, Supporting Information). The z-component electric field on the central axis $E_z((L+\mathrm{a})/2, L/2, z)$ is obtained by[10]:

$$E_z\left(\frac{L+a}{2},\ \frac{L}{2},\ z\right)$$
$$=-\frac{\sigma_U}{2\pi\varepsilon\,(\mathbf{r})}\left\{\arctan\frac{L\,(L+a)}{2\left(z-z_1\right)\sqrt{L^2+(L+a)^2+4\left(z-z_1\right)^2}}\right.$$
$$\left.+\arctan\frac{L\,(L-a)}{2\left(z-z_1\right)\sqrt{L^2+(L-a)^2+4\left(z-z_1\right)^2}}\right\}$$
$$+\frac{\sigma_T}{2\pi\varepsilon\,(\mathbf{r})}\left\{\arctan\frac{L\,(L+a)}{2\left(z-z_2\right)\sqrt{L^2+(L+a)^2+4\left(z-z_2\right)^2}}\right.$$
$$\left.+\arctan\frac{L\,(L-a)}{2\left(z-z_2\right)\sqrt{L^2+(L-a)^2+4\left(z-z_2\right)^2}}\right\}$$
$$-\frac{\sigma_T}{2\pi\varepsilon\,(\mathbf{r})}\left\{\arctan\frac{L\,(L+a)}{2\left(z-z_2\right)\sqrt{L^2+(L+a)^2+4\left(z-z_2\right)^2}}\right.$$
$$\left.+\arctan\frac{L\,(L-a)}{2\left(z-z_2\right)\sqrt{L^2+(L-a)^2+4\left(z-z_2\right)^2}}\right\}$$
$$+\frac{\sigma_U}{2\pi\varepsilon\,(\mathbf{r})}\left\{\arctan\frac{L\,(L+a)}{2\left(z-z_3\right)\sqrt{L^2+(L+a)^2+4\left(z-z_3\right)^2}}\right.$$
$$\left.+\arctan\frac{L\,(L-a)}{2\left(z-z_3\right)\sqrt{L^2+(L-a)^2+4\left(z-z_3\right)^2}}\right\}$$
$$-\frac{\sigma_E}{\pi\varepsilon\,(\mathbf{r})}\arctan\frac{L\,(L-a)}{2\left(z-z_1\right)\sqrt{L^2+(L-a)^2+4\left(z-z_1\right)^2}}$$
$$+\frac{\sigma_E}{\pi\varepsilon\,(\mathbf{r})}\arctan\frac{L\,(L-a)}{2\left(z-z_3\right)\sqrt{L^2+(L-a)^2+4\left(z-z_3\right)^2}} \tag{4}$$

where the surface charge densities are denoted as: σ_T, $-\sigma_T$ on the dielectric interface; σ_E, $-\sigma_E$ on the overlapping region and σ_U, $-\sigma_U$ on the nonoverlapping region of the electrode (Figure 2b), respectively. The corresponding positions are given by z_1, z_2, and z_3, respectively. Besides, the $a(t)$ represents the relative motion distance and L the length of the electrode/dielectric. When a resistor R is connected in the external circuit, the governing equation for the LS mode TENG is written as:

$$R\frac{\mathrm{d}}{\mathrm{d}t}\left[\sigma_E L\,(L-a)+\sigma_U La\right]=\int_{z_3}^{z_1}E_z\left(\frac{L+a}{2},\ \frac{L}{2},\ z\right)\mathrm{d}z \tag{5}$$

Sequentially, the average power output $P_{\mathrm{av,LS}}$ under a steady state can be calculated by:

$$P_{av,LS}=\frac{1}{T}\int_0^T R\left[L\left((L-a)\frac{\mathrm{d}\sigma_E}{\mathrm{d}t}+\left(\sigma_U-\sigma_E\right)\frac{\mathrm{d}a}{\mathrm{d}t}\right)\right]^2\mathrm{d}t \tag{6}$$

and similarly one can derive the best matching resistance for LS mode TENG by optimizing the average power output.

Solving the above equations, the transferred charges, voltage, current, and power can be numerically obtained. Most significantly, one can get the time-varying electric field of TENGs under different conditions, finally making full preparations for revealing the time-varying momentum distribution and whether the momentum is conserved in TENGs.

2.3. Momentum Current in TENGs

Momentum conservation in electrodynamics is not obvious since most electromagnetic field configurations carry linear

momentum. In addition, there is "hidden" mechanical momentum associated with the flow of current, for instance, in a general closed circuit. But locating the "hidden momentum" is not easy, and it is actually a relativistic effect.[27] Momentum current is a two-rank tensor which is the flow of momentum carried by matter with velocity, or it can only transmit momentum without the transfer of matter. The proof of momentum conservation is based heavily on the cancellation of internal forces in accordance with Newton's third law. As we will show, momentum conservation indeed holds true in TENGs as will be confirmed in the following sections.

The total electromagnetic force acting on the charges in a volume V is expressed by:

$$F_{mech} = \int_V (\mathbf{E} + \mathbf{v} \times \mathbf{B})\, \rho\, d\tau = \int_V (\rho \mathbf{E} + \mathbf{J} \times \mathbf{B})\, d\tau \tag{7}$$

where ρ is the electric charge density and $\boldsymbol{J}$ is the current density. Writing this equation in terms of fields, one has:

$$\mathbf{F}_{mech} = \int_V \left(-\varepsilon_0 \mu_0 \frac{\partial \mathbf{S}}{\partial t} + \nabla \cdot \overleftrightarrow{\mathbf{T}}\right) d\tau \tag{8}$$

where $\boldsymbol{S}$ is the Poynting vector defined by $\boldsymbol{S} = (\boldsymbol{E}\times\boldsymbol{B})/\mu_0$ representing the energy per unit time per unit area transferred by the electromagnetic (EM)-fields. The field $\overleftrightarrow{\mathbf{T}}$ is known as the Maxwell stress tensor defined as the force per unit area acting on the surface,

$$\overleftrightarrow{\mathbf{T}} = \varepsilon_0\, \mathbf{EE} + \frac{1}{\mu_0}\mathbf{BB} - \frac{1}{2}\left(\varepsilon_0 \mathbf{E}^2 + \frac{1}{\mu_0}\mathbf{B}^2\right)\mathbf{I} \tag{9}$$

which can also be written by T_{ij}, which is precisely the sum of the corresponding components of the electrostatic stress tensor $T_{ij}(\boldsymbol{E})$ and the magnetostatic stress tensor $T_{ij}(\boldsymbol{B})$:

$$\begin{aligned} T_{ij} &= T_{ij}\ (\mathbf{E}) + T_{ij}\ (\mathbf{B}) \\ &= \varepsilon_0\ \left(E_i E_j - \frac{1}{2}\delta_{ij}\mathbf{E}^2\right) + \frac{1}{\mu_0}\left(B_i B_j - \frac{1}{2}\delta_{ij}\mathbf{B}^2\right) \end{aligned} \tag{10}$$

where the Kronecker delta δ_{ij} is one if indices are the same ($\delta_{xx} = \delta_{yy} = \delta_{zz} = 1$) and zero otherwise ($\delta_{xy} = \delta_{yz} = \delta_{xz} = 0$). One index of T_{ij} states the direction of flow, while the other labels the components of the momentum. So, T_{ij} is the rate at which the j-th component of momentum flows through an area element oriented in the i direction or the rate at which the i-th component of momentum flows through an area element oriented in the j direction. Generally, if $\boldsymbol{S}$ does not vary in time or for quasi-static conditions, the total electromagnetic force on the charges in volume is calculated through the stress tensor at the boundary.

Newton's second law states that the net force on a system of particles is equal to the time derivative of the system's total mechanical linear momentum, $\boldsymbol{P}_{\mathbf{mech}}$. Therefore, Equation (8) can be rewritten as:

$$\mathbf{F}_{mech} = \frac{\mathrm{d}\mathbf{P}_{mech}}{\mathrm{d}t} = \int_V \left(-\varepsilon_0 \mu_0 \frac{\partial \mathbf{S}}{\partial t} + \nabla \cdot \overleftrightarrow{\mathbf{T}}\right) \mathrm{d}\tau \tag{11}$$

where $\boldsymbol{P}_{\mathbf{mech}}$ represents the total mechanical momentum of the charges within the volume V. The total linear momentum of the electric and magnetic fields in a volume V is:

$$\mathbf{P}_{em} = \varepsilon_0\, \mu_0 \int_V \mathbf{S}\, \mathrm{d}\tau = \varepsilon_0 \int_V \mathbf{E} \times \mathbf{B}\, \mathrm{d}\tau \tag{12}$$

Combining the above equations and using the divergence theorem:

$$\frac{\mathrm{d}\mathbf{P}_{total}}{\mathrm{d}t} = \frac{\mathrm{d}}{\mathrm{d}t}\ \left(\mathbf{P}_{mech} + \mathbf{P}_{em}\right) = \int_S \mathbf{n} \cdot \overleftrightarrow{\mathbf{T}} \mathrm{d}A \tag{13}$$

where the unit vector $\boldsymbol{n}$ is the normal vector to the area element dA. Thus, the statement of conservation of momentum in electrodynamics implies that the total momentum including both mechanical and electromagnetic contributions is equal to the momentum transferred by EM-fields. The momentum carried by EM fields themselves guarantees momentum conservation in electrostatics, magnetostatics, and electrodynamics. As with the charge conservation law, conservation of momentum can be expressed in a differential form. Equation (7) reveals that $\boldsymbol{F}_{\mathbf{mech}}$ is the volume integral of the Coulomb–Lorentz force density $\boldsymbol{f}_{\mathbf{mech}} = \rho\boldsymbol{E}+\boldsymbol{j}\times\boldsymbol{B}$. Since the integral volume V is arbitrary, a local conservation law of momentum is given by[27]:

$$\frac{\partial}{\partial t}\, \wp_{em} + \mathbf{f}_{mech} = \nabla \cdot \overleftrightarrow{\mathbf{T}} \tag{14}$$

where $\wp_{\mathrm{em}}$ is the electromagnetic momentum density defined by $\epsilon_0(\boldsymbol{E}\times\boldsymbol{B})$. It is important to note that the Poynting vector $\boldsymbol{S}$ plays two different roles: first it is interpreted as the energy current density transferred by EM-fields; and, second, it can be understood as the electromagnetic momentum density stored in the fields. Similarly, T_{ij} also plays two roles: T_{ij} represents the Maxwell electromagnetic stress acting on a surface, and it can be identified as the momentum current density transported by the fields.[27]

It is well known that the Maxwell stress tensor T_{ij} is a nine-component second-rank tensor of $\boldsymbol{E}$ and $\boldsymbol{B}$. In this work, we focus on the z-component of the momentum and the electromagnetic force, therefore we provide the detailed expressions for T_{zj}:

$$T_{zx} = \varepsilon_0\, E_z E_x + \frac{1}{\mu_0} B_z B_x \tag{15}$$

$$T_{zy} = \varepsilon_0\, E_z E_y + \frac{1}{\mu_0} B_z B_y \tag{16}$$

$$T_{zz} = \frac{\varepsilon_0}{2}\ \left(E_z^2 - E_x^2 - E_y^2\right) + \frac{1}{2\mu_0}\left(B_z^2 - B_x^2 - B_y^2\right) \tag{17}$$

where T_{zx}, T_{zy}, and T_{zz} represent the z component of momentum oriented from the x, y, and z direction, respectively (the x- and y-components of Maxwell stress tensor are presented in Section S3, Supporting Information). Because the magnetic induction $\boldsymbol{B}$ is close to zero when dealing with $\wp_{\mathrm{em}}$ in Equations (9–14) under quasi-static condition, hence,

$$T_{ij} = \varepsilon_0\ \left(E_i E_j - \frac{1}{2}\delta_{ij}\mathbf{E}^2\right) \tag{18}$$

$$T_{zx} = \varepsilon_0 E_z E_x \tag{19}$$

$$T_{zy} = \varepsilon_0 E_z E_y \tag{20}$$

$$T_{zz} = \frac{\varepsilon_0}{2}\left(E_z^2 - E_x^2 - E_y^2\right) \tag{21}$$

Furthermore, based on Equation (8) the total electromagnetic force on a volume V is evidently:

$$\mathbf{F} = \int_V \nabla \cdot \overleftrightarrow{\mathbf{T}} \mathrm{d}\tau \tag{22}$$

By using the divergence theorem, the above equation is changed to:

$$\mathbf{F} = \oint_S \mathbf{n} \cdot \overleftrightarrow{\mathbf{T}} \mathrm{d}A \tag{23}$$

which shows that the total force acting on the volume V is equal to the surface integral of the stress tensor bounded by a closed surface S (Gaussian surface) of the volume (Figure 2c). Assuming a cuboid Gaussian surface enclosed with six finite planes: $x = x_0$, $x = x_1$, $y = y_0$, $y = y_1$, $z = z_0$, $z = z_1$, the z-component of electromagnetic force F_z becomes:

$$F_z = \Gamma^{\square}_{up} - \Gamma^{\square}_{down} + \Gamma^{\square}_{front} - \Gamma^{\square}_{behind} + \Gamma^{\square}_{right} - \Gamma^{\square}_{left} \tag{24}$$

where,

$$\begin{aligned}\Gamma^{\square}_{up} &= \int_{y_0}^{y_1}\int_{x_0}^{x_1} T_{zz}\left(x, y, z_1\right)\mathrm{d}x\mathrm{d}y \\ &= \int_{y_0}^{y_1}\int_{x_0}^{x_1} \frac{\varepsilon(\mathbf{r})}{2}\Big(E_z\left(x, y, z_1\right)^2 - E_x\left(x, y, z_1\right)^2 \\ &\quad - E_y\left(x, y, z_1\right)^2\Big)\mathrm{d}x\mathrm{d}y\end{aligned} \tag{25}$$

$$\begin{aligned}\Gamma^{\square}_{down} &= \int_{y_0}^{y_1}\int_{x_0}^{x_1} T_{zz}\left(x, y, z_0\right)\mathrm{d}x\mathrm{d}y \\ &= \int_{y_0}^{y_1}\int_{x_0}^{x_1} \frac{\varepsilon(\mathbf{r})}{2}\Big(E_z\left(x, y, z_0\right)^2 - E_x\left(x, y, z_0\right)^2 \\ &\quad - E_y\left(x, y, z_0\right)^2\Big)\mathrm{d}x\mathrm{d}y\end{aligned} \tag{26}$$

$$\begin{aligned}\Gamma^{\square}_{front} &= \int_{z_0}^{z_1}\int_{x_0}^{x_1} T_{yz}\left(x, y_1, z\right)\mathrm{d}x\mathrm{d}z \\ &= \int_{z_0}^{z_1}\int_{x_0}^{x_1} \varepsilon(\mathbf{r})\, E_y\left(x, y_1, z\right) E_z\left(x, y_1, z\right)\mathrm{d}x\mathrm{d}z\end{aligned} \tag{27}$$

$$\begin{aligned}\Gamma^{\square}_{behind} &= \int_{z_0}^{z_1}\int_{x_0}^{x_1} T_{yz}\left(x, y_0, z\right)\mathrm{d}x\mathrm{d}z \\ &= \int_{z_0}^{z_1}\int_{x_0}^{x_1} \varepsilon(\mathbf{r})\, E_y\left(x, y_0, z\right) E_z\left(x, y_0, z\right)\mathrm{d}x\mathrm{d}z\end{aligned} \tag{28}$$

$$\begin{aligned}\Gamma^{\square}_{right} &= \int_{z_0}^{z_1}\int_{y_0}^{y_1} T_{xz}\left(x_1, y, z\right)\mathrm{d}y\mathrm{d}z \\ &= \int_{z_0}^{z_1}\int_{y_0}^{y_1} \varepsilon(\mathbf{r})\, E_x\left(x_1, y, z\right) E_z\left(x_1, y, z\right)\mathrm{d}y\mathrm{d}z\end{aligned} \tag{29}$$

$$\begin{aligned}\Gamma^{\square}_{left} &= \int_{z_0}^{z_1}\int_{y_0}^{y_1} T_{xz}\left(x_0, y, z\right)\mathrm{d}y\mathrm{d}z \\ &= \int_{z_0}^{z_1}\int_{y_0}^{y_1} \varepsilon(\mathbf{r})\, E_x\left(x_0, y, z\right) E_z\left(x_0, y, z\right)\mathrm{d}y\mathrm{d}z\end{aligned} \tag{30}$$

where $\Gamma^{\square}_{up}$, $\Gamma^{\square}_{down}$, $\Gamma^{\square}_{front}$, $\Gamma^{\square}_{behind}$, $\Gamma^{\square}_{right}$, $\Gamma^{\square}_{left}$ represents the momentum current flowing through the corresponding up, down, front, behind, and left surface of the cuboid, respectively (the x- and y-components of electromagnetic force are presented in Section S3, Supporting Information). It is indisputable that the total electromagnetic force and momentum current on the charges do not change in the presence of EM-fields, but one should ensure that the total charge enclosed by the volume remains unchanged. Therefore, as exhibited in Figure 2c, the Gaussian surface tightly packaging the dielectrics can be extended and is equivalent to two infinite parallel planes perpendicular to the z-axis plus four finite planes being parallel to the z-axis.

In Figure 2d,e, a set of infinite parallel planes are placed on both sides of the dielectrics and electrodes of TENGs. The surface integration of the z-component momentum current density over the i-th infinite plane negative toward the z-axis is denoted as Γ^{∞}_i; while the subtraction of Γ^{∞}_i and Γ^{∞}_j is the change of momentum current $\Delta\Gamma$ on particles sandwiched between the i-th and j-th infinite parallel planes:

$$\begin{aligned}\Gamma^{\infty}_i &= \iint T_{zz}\mathrm{d}x\mathrm{d}\left(x, y, z_i\right)y \\ &= \int_{-\infty}^{+\infty}\int_{-\infty}^{+\infty} \frac{\varepsilon(\mathbf{r})}{2}\Big(E_z\left(x, y, z_i\right)^2 - E_x\left(x, y, z_i\right)^2 \\ &\quad - E_y\left(x, y, z_i\right)^2\Big)\mathrm{d}x\mathrm{d}y\end{aligned} \tag{31}$$

Taking Figure 2d as an example, there are eight infinite parallel planes setting up previously to calculate the momentum current

passing through the electrodes and dielectrics of the CS mode TENG:

$$\Delta\Gamma_{elec1} = \Gamma_1^{\infty} - \Gamma_2^{\infty} \quad (32)$$

$$\Delta\Gamma_{die1} = \Gamma_2^{\infty} - \Gamma_4^{\infty} \quad (33)$$

$$\Delta\Gamma_{up} = \Gamma_1^{\infty} - \Gamma_4^{\infty} \quad (34)$$

$$\Delta\Gamma_{die2} = \Gamma_5^{\infty} - \Gamma_7^{\infty} \quad (35)$$

$$\Delta\Gamma_{elec2} = \Gamma_7^{\infty} - \Gamma_8^{\infty} \quad (36)$$

$$\Delta\Gamma_{down} = \Gamma_5^{\infty} - \Gamma_8^{\infty} \quad (37)$$

Using the same method, seven infinite parallel planes are set up to describe the momentum current distribution and variation in the LS mode TENG (Figure 2e). Note that there is no air gap between the two dielectric materials. As a result, one parallel plane is reduced when compared with the CS mode TENG.

3. Results and Discussion

Numerical experiments are carried out to clarify the time-varying momentum distribution and reveal whether the momentum is conserved in TENGs. The relevant configurations, derived equations, and schematic diagrams as well as the variation of momentum current under SC condition are demonstrated in Figure 2. Figure 2a illustrates the basic configuration, materials, and surface charge density of the CS mode TENG in a Cartesian coordinate system, whose x–z section is depicted in Figure 2d with eight infinite parallel planes. Likewise, the basic configuration and x–z section with seven surfaces of the LS mode TENG are exhibited in Figure 2b,e, respectively. Several key formulas are listed in Figure 2f. Taking the CS mode TENG as an example, the change of momentum current density in a complete operation cycle under SC condition are presented in Figure 2g. Its sub-graphs g1, g2, g3 visualize the distribution of momentum current at the beginning, a quarter, and half a period, respectively. An interesting find is that the configuration of momentum current distribution close to the charges on electrodes and dielectrics remain relatively constant, while they change violently in the air gap during the periodic movement of the CS mode TENG.

Momentum current Γ_i^{∞} downward along the z-axis through eight infinite parallel planes are depicted in **Figure 3**, under short circuit (SC), open circuit (OC), and optimum load conditions, respectively. Figure 3a illustrates the variation of momentum current Γ_i^{∞} passing through eight surfaces that are placed around the CS model TENG. It is interestingly observed that the momentum current flowing in the surface 2 (Γ_2^{∞}), and surface 3 (Γ_3^{∞}), are exactly equal with each other. A similar phenomenon can also be found from the surface 4 (Γ_4^{∞}), and surface 5 (Γ_5^{∞}), which are set in the air gap; and the surface 6 (Γ_6^{∞}), and surface 7 (Γ_7^{∞}) that are placed in the dielectric 2. The momentum current can be absorbed by the dielectrics. Note that the momentum change crossing the dielectric 1 ($\Delta\Gamma_{die1}$, calculated by $\Gamma_2^{\infty} - \Gamma_4^{\infty}$) and dielectric 2 ($\Delta\Gamma_{die2}$, calculated by $\Gamma_5^{\infty} - \Gamma_7^{\infty}$) have the same magnitude but changes in opposite directions (Figure 3b,c). This is because the absorbed momentum by the dielectrics produces a recoil force such that the system is maintained in equilibrium. This reflects that an external force applied to one dielectric in equilibrium is reacted by the internal force (recoil force) produced within the dielectric. So, the momentum current delivered to (absorbed by) the moving part ($\Delta\Gamma_{up}$) is equal to that of absorbed by (delivered to) the down part ($\Delta\Gamma_{down}$). As a result, the general conclusion is that the momentum is conserved in the TENGs system as a whole at SC conditions. We also note that the momentum currents in the z direction passing the surface 1 (Γ_1^{∞}), and 8 (Γ_8^{∞}) are negligible. This is mainly because the transmission of momentum current is interrupted by the free charges distributed in the electrodes; or simply, the total quasi-electrostatic field outside the TENG device is almost completely shielded owing to the metal electrode, particularly the distribution of induced charges within it.

Results depicted in Figure 3d–g indicate that the momentum changes either absorbed by the dielectric 1 ($\Delta\Gamma_{die1}$) and dielectric 2 ($\Delta\Gamma_{die2}$), or the up part ($\Delta\Gamma_{up}$) and down part ($\Delta\Gamma_{down}$) of the TENG, are equal but change in the opposite direction (Figure 3e–g), once again suggesting that the momentum is conserved in TENGs. However, the momentum current passing the surface 4 (Γ_4^{∞}) (and the surface 5 (Γ_5^{∞}) becomes gently compared to the SC conditions (Figure 3a,d). This primarily attributes to the fact that no charges are transferred between the two electrodes at OC conditions, thus the electric field generated by the triboelectric charges cannot be thoroughly shielded, leading to a small impact on the variation of momentum current within the air gap.

To maximize power output of the CS mode TENG, an optimum resistance is loaded. At this time, except for the variations of momentum currents crossing the surface 4 (Γ_4^{∞}) and surface 5 (Γ_5^{∞}), the momentum changes crossing other surfaces are similar to those of under SC conditions (Figure 3g,h). This is because only part of the electric field is shielded by the free charges distributed on the electrodes during the CS process. As a result, the peak of momentum in the z direction crossing the surface 4 (and/or surface 5) is smaller than that of obtained at SC conditions but it is larger than that under OC conditions. Moreover, as presented in Figure 3a, these time curves are spontaneously divided into four groups: $A(\Gamma_2^{\infty}, \Gamma_3^{\infty})$, $B(\Gamma_4^{\infty}, \Gamma_5^{\infty})$, $C(\Gamma_6^{\infty}, \Gamma_7^{\infty})$ and $D(\Gamma_1^{\infty}, \Gamma_8^{\infty})$, according to their different physical surroundings. Although the changing trends of momentum current in different groups possess different forms, they have obvious similar characteristics. This is the reason why each curve within the group exactly overlaps with each other. Note that the momentum current passing through surface 1 (or surface 8) placed outside the TENG device indeed is negligible.

Even subject to different loading conditions, the total momentum imparted to the up part $\Delta\Gamma_{up}$ and down part $\Delta\Gamma_{down}$ of the TENG device is equal to each other (**Figure 4**a,c). As the loaded resistor increases, fluctuation of $\Delta\Gamma_{up}$ and $\Delta\Gamma_{down}$ gradually decreases, while the peaks extracted from the momentum currents ($\Delta\Gamma_{up,peak}$, and $\Delta\Gamma_{down,peak}$) get smaller (Figure 4b). On the other hand, increasing the external loaded resistors also cause a phase lag problem, which is evident in the red shadow in Figure 4a and the corresponding enlarged image in Figure 4e. For a larger resistor, phase delay begins to increase significantly. However, the phase recovers at OC conditions since at this point the frequency of time-varying electric field must be strictly consistent with the external mechanical excitation. The total momentum must be

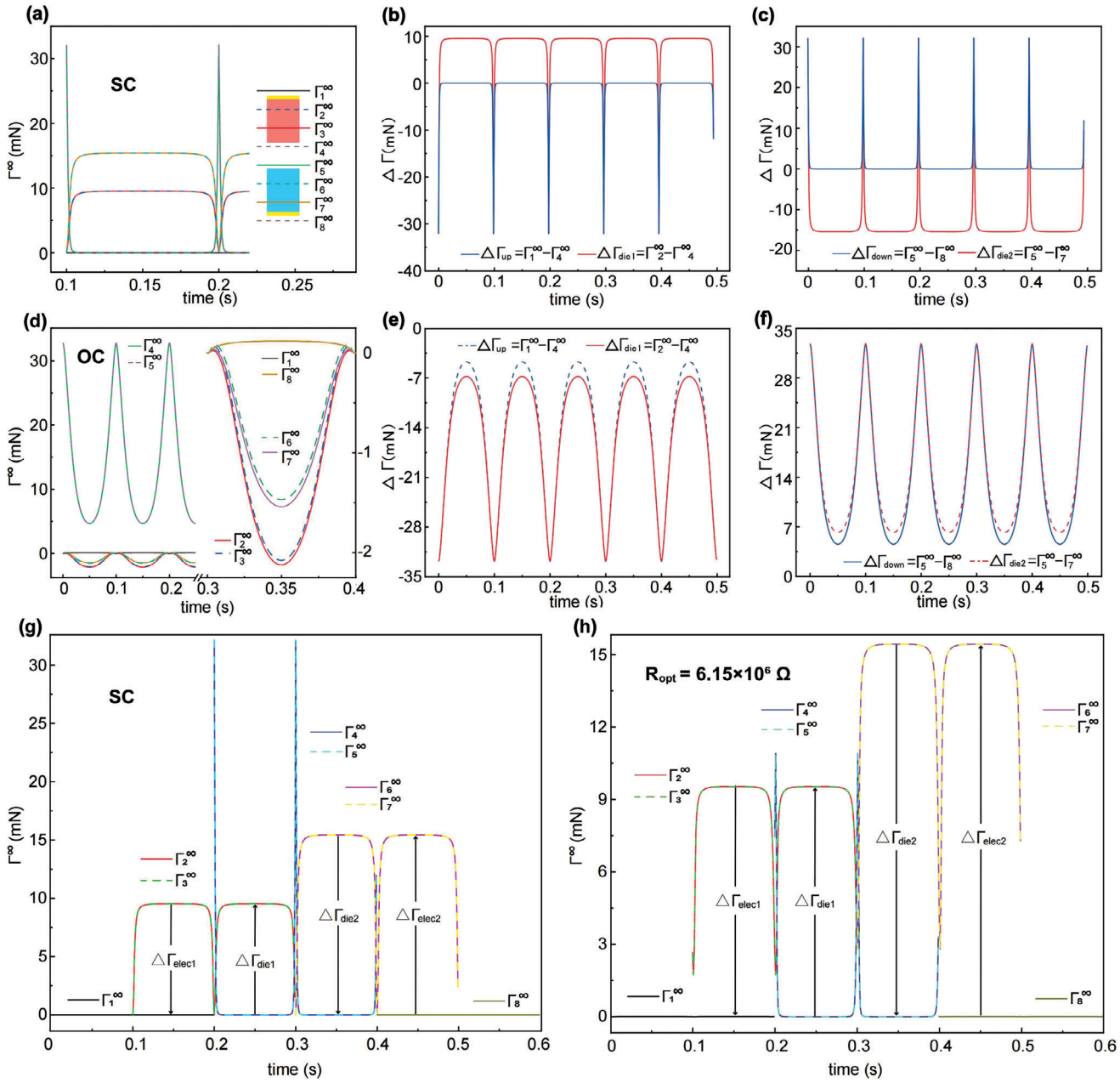

Figure 3. Momentum current and momentum change of contact-separation mode TENG. a) Under short circuit (SC) condition, theoretically calculated momentum current passing through eight infinite planes negative toward the *z*-axis, b) momentum change between two infinite planes on either side of dielectric 1 and the moving (top) part, c) dielectric 2 (die 2) and the stationary (down) part of the contact-separation mode TENG device. Inset in (a): distribution of eight infinite planes perpendicular to the *z*-axis. d) Under open circuit (OC) condition, theoretically calculated momentum current passing through eight infinite planes negative toward the *z*-axis, e) momentum change between two infinite planes on either side of dielectric 1 and the moving part, f) dielectric 2 and the stationary part. g) Time-varying momentum current through eight infinite planes under short circuit (SC) condition, and h) optimum resistor condition.

zero if we only consider the electromagnetic momentum originally stored in the field. It is worth highlighting that when the center of mass of a localized system is at rest, its total momentum must be zero, meaning that the net force on this system is zero. Exploiting this fact, analyzing the force situation of the TENGs has implications in understanding the law of variation for momentum current. As stated before, if the momentum is absorbed by the moving part (or stationary part) a recoil force is generated. Note that the generated recoil force is an internal force. According to Newton's second law, the force on an object is equal to the rate of change of its momentum. In other words, a zero external force results in an invariant momentum. Observe that momentum conservation in the system from can also be obtained by calculating the total electromagnetic force acting on the TENG.

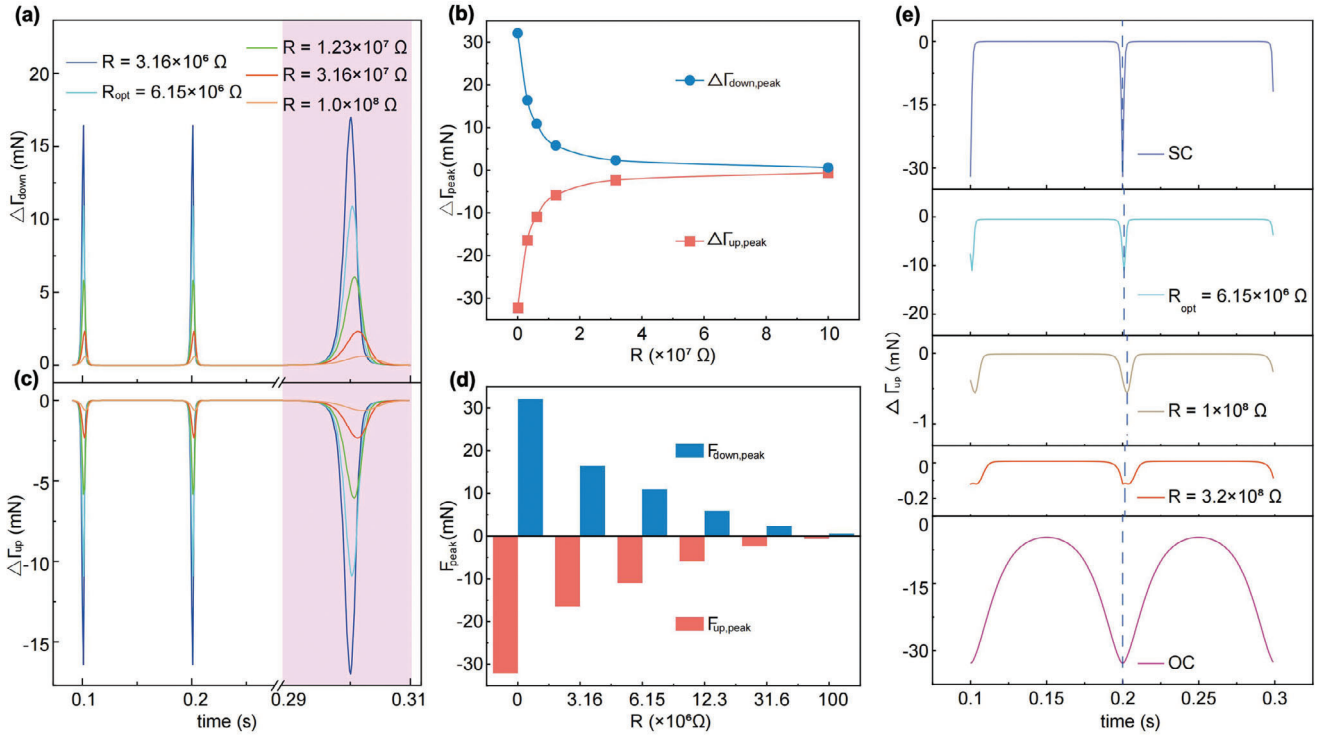

Figure 4. Time-varying momentum current under different loading conditions. The total momentum imparted to the a) moving part ($\Delta\Gamma_{up}$) and c) stationary part ($\Delta\Gamma_{down}$) of the contact-separation mode TENG device. b) The corresponding peaks of $\Delta\Gamma_{up}$ and $\Delta\Gamma_{down}$. d) The peaks of electromagnetic force acting on the moving part ($F_{up,peak}$) and stationary part ($F_{down,peak}$), respectively. e) Time-varying momentum current under short circuit (SC), different loading resistors, and open circuit (OC) conditions, respectively.

Generally, there are two classical ways to determine the electromagnetic force: one way is by virtue of momentum conservation since the force acting on an object is equal to the rate of change of its momentum; another approach is using the Coulomb–Lorentz force density $\boldsymbol{f}_{\mathbf{mech}} = \rho\boldsymbol{E}+\boldsymbol{j}\times\boldsymbol{B}$. Using the first way, the recoil force can be calculated; because it is the result of total flowing momentum absorbed by an object; alternatively through considering the stress tensor (force per unit area) acting on a surface, the total electromagnetic force acting on an object can also be obtained. Figure 4d illustrates the variation of the force peak acting on the up part ($F_{up,peak}$) and down part ($F_{down,peak}$) for different loading conditions. **Figure 5** depicts the time-dependence of the z-component of the electromagnetic force (F_z) at SC and OC conditions as calculated according to Equation (24). As expected, both the z-component of electromagnetic force F_z acting on the up part (F_{up}) and down part (F_{down}) of the CS model TENG are equal and opposite whether at SC conditions (Figure 5a) or OC conditions (Figure 5c). Here the momentum current passing these planes is denoted as $\Gamma^{\square}$. Simply, the F_z is calculated by the momentum crossing the up ($\Gamma^{\square}_{u}$), down ($\Gamma^{\square}_{d}$), front ($\Gamma^{\square}_{f}$), behind ($\Gamma^{\square}_{b}$), left ($\Gamma^{\square}_{l}$), and right ($\Gamma^{\square}_{r}$) surfaces, where the six defined finite surfaces are inserted in Figure 5b1 forming a Gaussian surface. Numerical results (Figure 5b,d) indicate that the momentum current mainly comes from the down ($\Gamma^{\square}_{d}$) surface which plays a major contribution to F_{up} both at SC and OC conditions. As stated before, the momentum current crossing a surface of one object is essentially the electromagnetic force acting on this surface. In other words, the largest Maxwell stress tensor is applied on the down surface of the up part of the CS model TENG, due to large number of triboelectric charges uniformly distributed on the contacting surfaces that are parallel to the down surface and perpendicular to the z direction.

Unsurprisingly, the momentum absorbed by the moving part and stationary part of the LS model TENG are equal to each other, but with an opposite changing tendency (**Figure 6**a,b,d,e). The momentum crossing through the surface 1 (Γ^{∞}_{1}) and surface 7 (Γ^{∞}_{7}) is almost negligible which is similar to that of in the CS model TENG. However, the magnitude of $\Delta\Gamma_{up}$ obtained at SC conditions is much larger than that obtained under OC conditions which is caused by the different momenta at surface 4 (Γ^{∞}_{4}) (Figure 6c,f,h). This phenomenon must be understood in the following way. At SC conditions, the charge density (σ_E and $-\sigma_E$ in Equation 4) distributed at the overlapping region of the electrode is approximately zero, because this region is electrically neutral. Thus, the total electric field distributed at the overlapping regions of the two dielectric is insignificant, a fact which was demonstrated in Refs.[3,11,12] Besides, although the triboelectric charges are created uniformly at the nonoverlapping regions of the dielectrics, the generated corresponding electric field can be shielded by the free charges that are induced at the nonoverlapping regions of the electrodes. Even so, one can still observe a high electric field from the nonoverlapping regions. As a result, there is a larger momentum current flowing through the surface 4 Γ^{∞}_{4} when compared to the momentum flowing through other surfaces at SC conditions. Nevertheless, at OC conditions the induced charges are all accumulated at the overlapping regions,

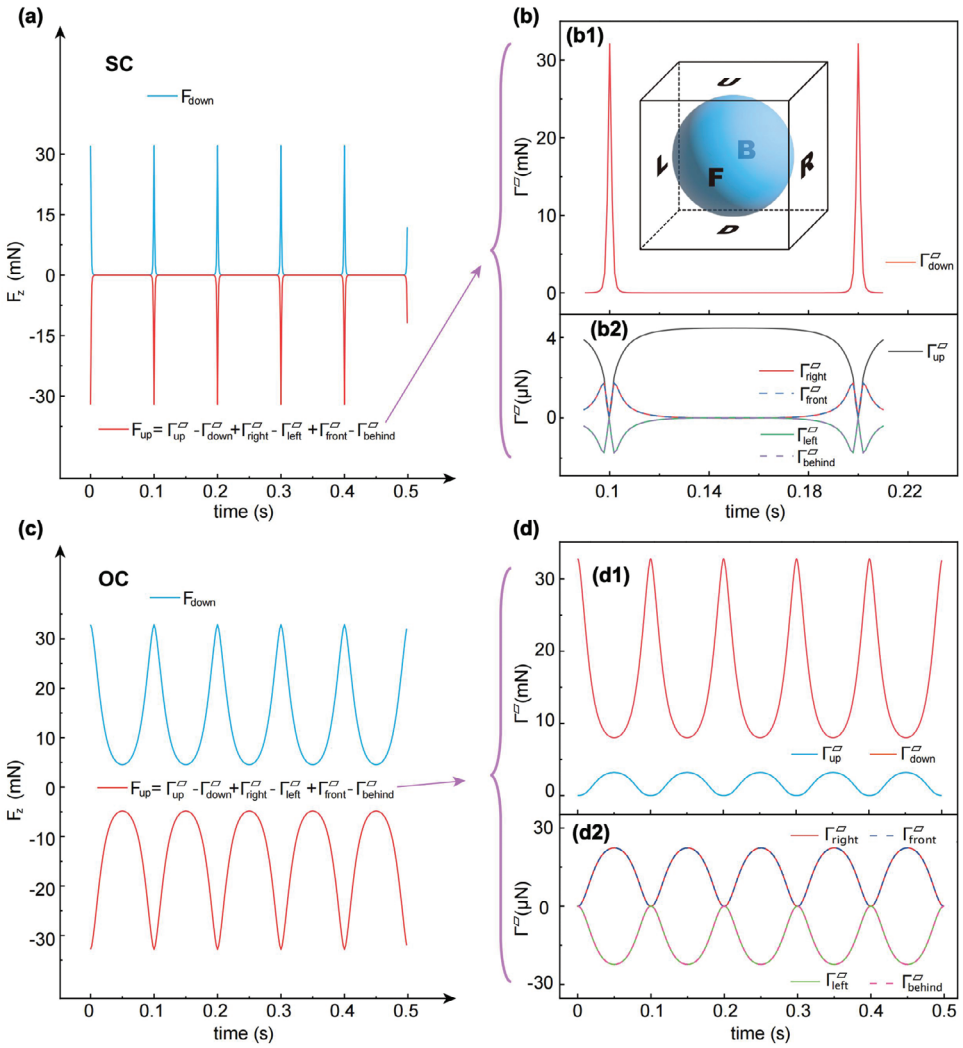

Figure 5. Time-varying electromagnetic force acting on the contact-separation mode TENG device calculated through momentum current. Theoretically calculated the *z*-component of electromagnetic force acting on the up (F_{up}) and down part (F_{down}) of the TENG device, under a) SC, and c) OC conditions, respectively. b) Momentum current through the downward (b1), upper, frontage, backward, left and right (b2) side finite plane negative toward the *z*-axis, composing the electromagnetic force acting on the up part at SC condition. Inset in (b1): an example of Gaussian surface bounded by six finite planes. d) Momentum current through the upper, downward (d1), frontage, backward, left and right (d2) side finite plane negative toward the *z*-axis, composing the electromagnetic force acting on the up part at OC condition.

which have to remain a neutral state of the electrode since there is no charge transferred. Consequently, as the relative displacement increases, much more induced charges are accumulated at the overlapping regions of the electrodes, thereby generating an increasing electric field and thus an increasing momentum current flowing through the surface 4 (Γ_4^{∞}). This is also the reason why there is a much larger Γ_4^{∞} obtained at OC conditions than it at SC conditions. Figure 6h displays a clear picture of momentum current flowing through seven different surfaces that are illustrated in Figure 6f. When an optimum resistor is loaded, the variation of momentum currents are shown in Figure 6g.

Additionally, the momentum stored in the up part ($\Delta\Gamma_{up}$) and down part ($\Delta\Gamma_{down}$) of the LS TENG at different loading conditions (**Figure** 7a,c) suggests that the total momentum is zero; that is, momentum is conserved. Once again one exactly confirms conservation of momentum. As the external resistor increases, a phase difference of momentum appears which is clearly observed from an expanded image inserted in Figure 7a; while the relevant momentum current peaks gradually increases (Figure 7b). The details of phase-leading and peak-increasing are demonstrated in Figure 7e. Furthermore, the peak of the electromagnetic force acting on the up part ($F_{up,peak}$) and down part ($F_{down,peak}$) also gradually increases as the resistance increases (Figure 7d). **Figure 8** depicts the relationship between the electromagnetic fore F_z and momentum current of the LS mode TENG. It is easily found that the up part experiences exactly the same force (F_{up}) as the down part (F_{down}) but in opposite directions whether at SC condition or loaded conditions (Figure 8a,c). Consider now the moving part (up part). The same momentum currents flow into the up surface ($\Gamma_{up}^{\square}$) and down surface ($\Gamma_{down}^{\square}$), respectively (the inset image illustrated in Figure 8a); but they change in an opposite direction (Figure 8b).

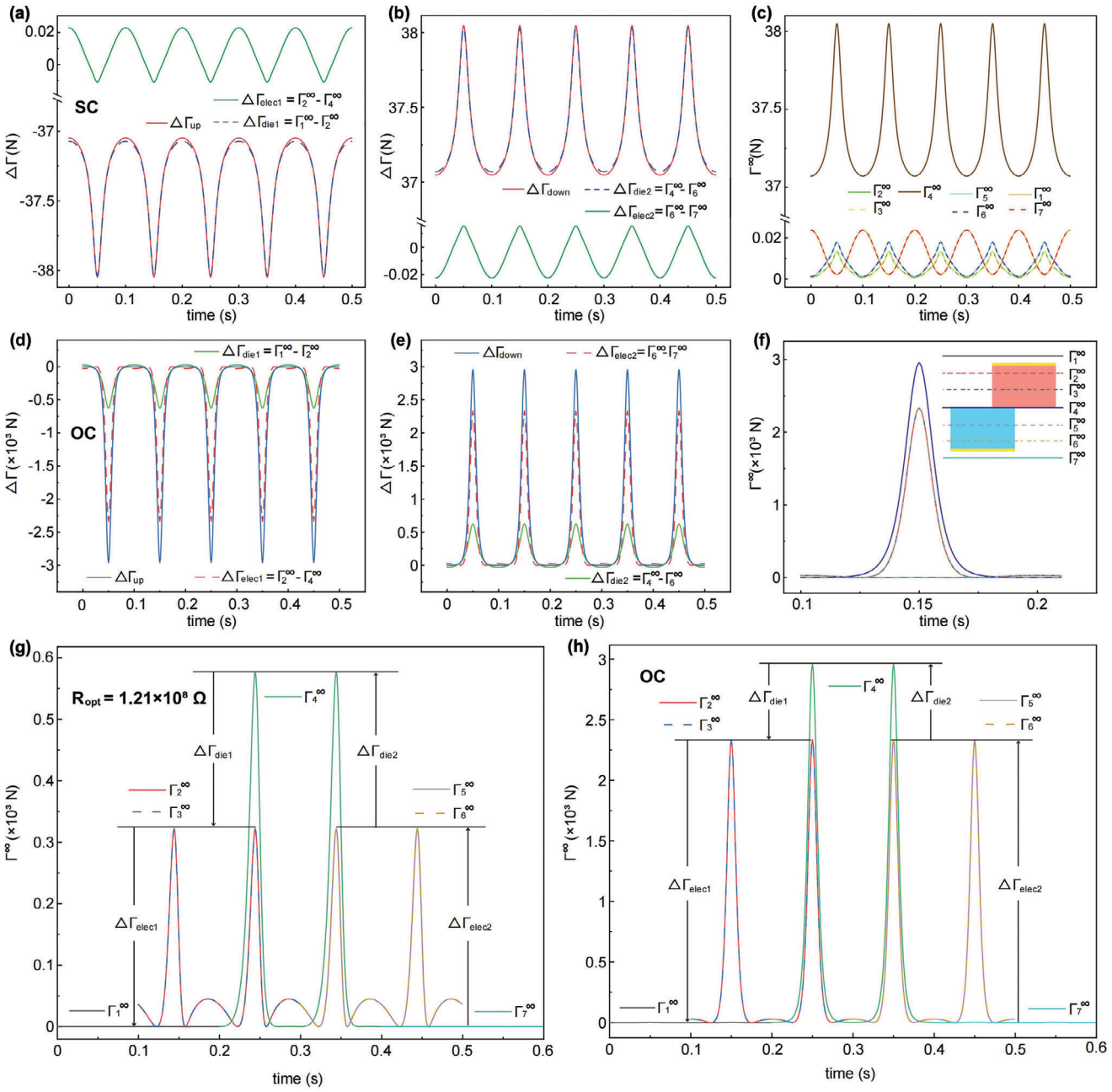

Figure 6. Time-varying momentum current of the lateral-sliding mode TENG at different conditions. Under short circuit (SC) condition, theoretically calculated momentum current passing through the a) up (moving) part, b) the down (stationary) part, and c) the seven infinite planes negative toward the *z*-axis of the lateral-sliding mode TENG device, respectively. Under open circuit (OC) condition, theoretically calculated momentum current passing through the d) up (moving) part, e) the down (stationary) part, and f) the seven infinite planes negative toward the *z*-axis of the lateral-sliding mode TENG device, respectively. Inset in (f): distribution of seven infinite planes perpendicular to the *z*-axis. Time-varying momentum current passing through seven infinite planes under g) optimum resistor (R_{opt}) condition and h) open circuit (OC) condition (h), respectively.

The above phenomenon is quite different from that of the CS model TENG, as in the latter case there is almost no momentum current crossing through the up surface (Figure 5b). This phenomenon in LS mode TENG is mainly due to the electric field generated by the triboelectric charges distributed at the nonoverlapped regions of the dielectrics (Figure 2b,e). At SC conditions, when there is a relative displacement, free charges are induced and distributed at the nonoverlapped region of the electrodes; and the shielding charges have opposite sign but are equal to the triboelectric charges. As a result, the same amount of momentum will flow into or out through the nonoverlapped regions. If an external resistor is loaded, the flow speed of charges transferred between the two electrodes is mainly affected, but does not influence the result. As depicted in Figure 8c, the F_{up} acting

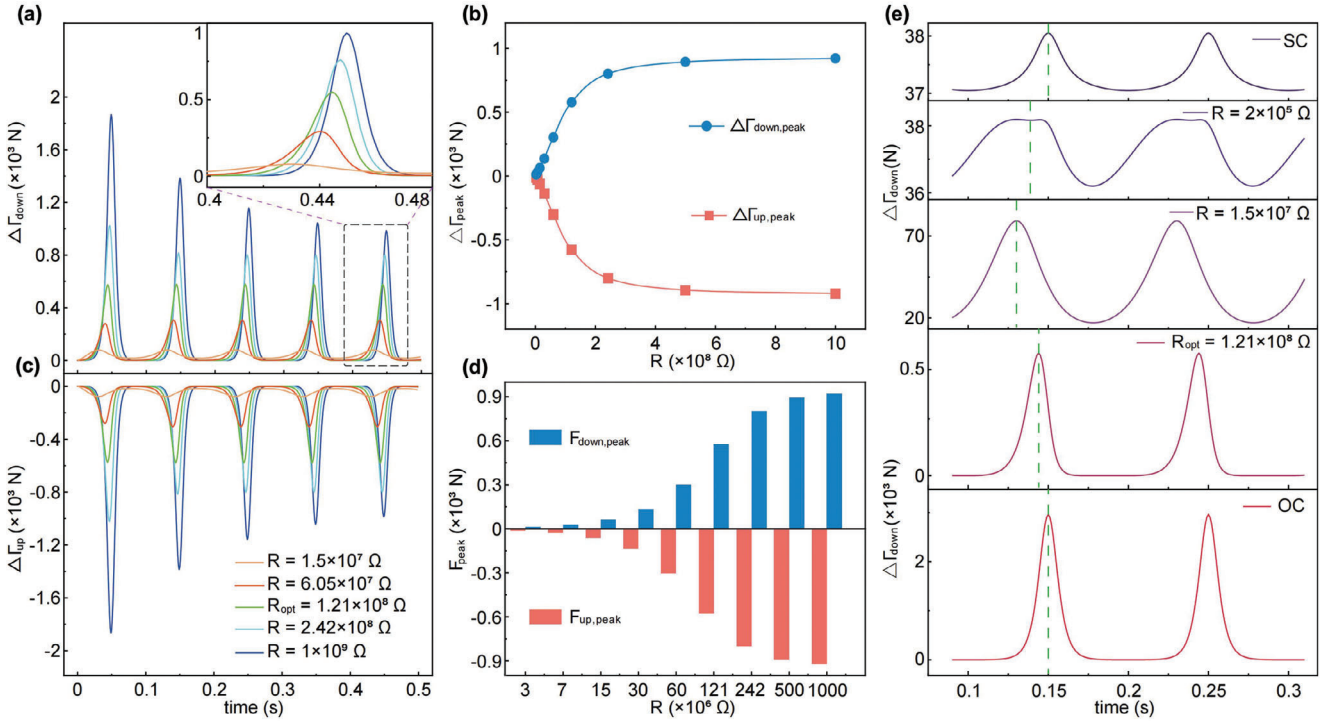

Figure 7. Time-varying momentum current under different loading conditions of the lateral-sliding mode TENG. The total momentum imparted to the a) down (stationary) part ($\Delta\Gamma_{down}$) and c) up (moving) part ($\Delta\Gamma_{up}$) of the lateral-sliding mode TENG device. b) The corresponding peaks of $\Delta\Gamma_{down,peak}$, and $\Delta\Gamma_{up,peak}$ respectively. d) The peaks of electromagnetic force acting on the moving part ($F_{up,peak}$) and stationary part ($F_{down,peak}$), respectively. e) Time-varying momentum current under short circuit (SC), different loading resistors, and open circuit (OC) conditions, respectively.

on the moving part is equal to the force acting on the stationary part (F_{down}), but with an opposite direction under loaded an optimum resistor. One important aspect to note is that the momentum flowing through the down surface ($\Gamma^{\square}_{down}$) exhibits a main contribution to F_{up} (Figure 8d); here the reason behind is similar to the previous observation that most of the momentum flows through the surface 4 (Γ^{∞}_{4}) at OC conditions (Figure 6h). Numerical results stress again that the momentum currents flowing into a volume is equal to the resultant external force acting on the system. Consequently, momentum conservation is validated once again in a TENG device.

4. Conclusion

In this work, the time-varying momentum transfer and distribution within the TENGs are systematically analyzed through a time-dependent 3D mathematical model. After exploring the absorption and impartation of momentum by field and dielectric materials, it is revealed that the energy harvesting system based on TENGs shows momentum conservation. A TENG device can not only convert mechanical energy into electrical energy, but also transfer momentum. In other words, momentum transfer is one of the important characteristic of TENGs, and the energy harvesting system based on TENGs is also a momentum transfer system. Momentum will remain unchanged all along the time within the whole system or transfer somewhere when there is no net external force. This character of TENG promises applications in some special area which will be explored hereafter. The basic conclusions are as follows:

i. The momentum currents either absorbed by the moving part ($\Delta\Gamma_{up}$), or the stationary part ($\Delta\Gamma_{down}$) of a TENG, are equal in magnitude but opposite in direction. Increasing the load resistance, the peaks of the $\Delta\Gamma_{up}$ and $\Delta\Gamma_{down}$ gradually smaller, and also leads to a phase lag when the TENG device is operated under a steady state. The exhibited symmetry between $\Delta\Gamma_{up}$ and $\Delta\Gamma_{down}$ all along the process once again indicates the conservation of momentum.
ii. The total electromagnetic force acting on a volume V is equal to the surface integral of the stress tensor bounded by a closed surface S (Gaussian surface) of the volume, which is also exactly equivalent to the momentum current passing through the Gaussian surface of the volume. Thus, it is understood quite easily that the electromagnetic forces acting on the moving part and stationary part of TENGs are equal with each other but acting in a contrary direction. Therefore, a working TENG device remains in static equilibrium not because there are no electrostatic forces acting on it but because these forces annihilate one another.
iii. The momentum current flowing into a volume is equal to the resultant external force acting on the system. When the momentum is absorbed by the moving part or stationary part of a TENG a recoil force is generated. This generated force is an internal force. More generally, the total electromagnetic force and total momentum current on the charges transmitted by the field do not vary as the volume V and the surrounding Gaussian surface change if that the total quantity of charges encircled by the volume surface remains constant. Note that the total momentum of a TENG is zero under any conditions,

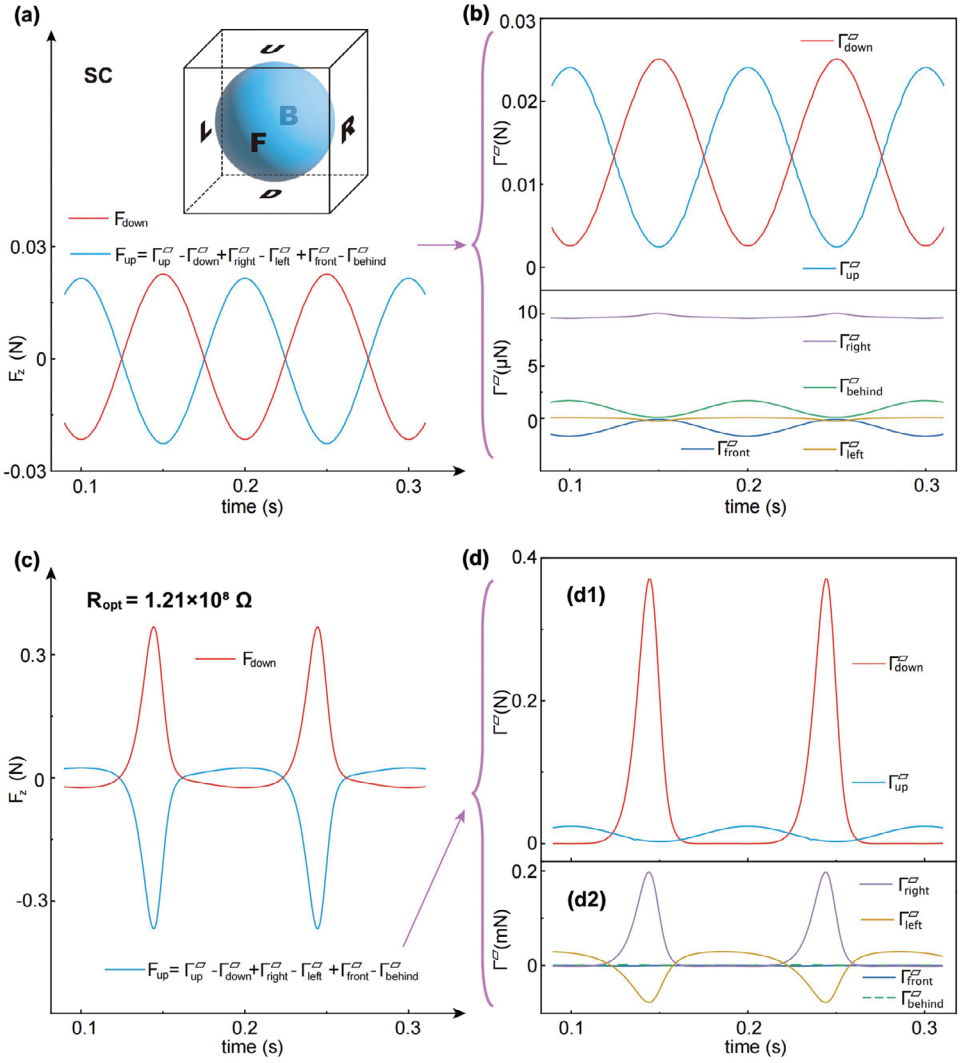

Figure 8. Time-varying electromagnetic force acting on the lateral-sliding mode TENG device calculated through momentum current. Theoretically calculated the *z*-component of electromagnetic force acting on the up (F_{up}) and down part (F_{down}) of the TENG device, under a) SC, and c) optimum resistance (R_{opt}) condition, respectively. Inset in (a): six finite planes composing a Gaussian surface. b) Momentum current through the upper, downward, frontage, backward, left and right side finite plane negative toward the *z*-axis, composing the electromagnetic force acting on the up part of the TENG device at SC condition. d) Momentum current through the upper, downward (d1), frontage, backward, left, and right (d2) side finite plane negative toward the *z*-axis, composing the electromagnetic force acting on the up part of the TENG device at R_{opt} condition.

mainly because of the electrical neutrality of the TENG. Exploiting this fact, it is easy to ascertain why the total electrostatic forces acting on TENGs must be zero.

iv. The free (induced) charges distributed on the electrodes can shield the propagation of the electric field and consequently interrupt the transmission of momentum current. Under OC conditions, the shielding effect decreases so that the momentum fluctuation flats as there are no free charges transferred between the electrodes of TENGs. In the case of SC conditions, the momentum currents absorbed either by the stationary part or moving part of TENGs will be completely shielded, giving rise to a severe momentum fluctuation due to transfer of the induced charge. For all cases, it is assumed that the TENG is operated under a low working frequency. However, if the operation frequency increases to the MHz or GHz range, a dynamic magnetic field as well as the Poynting vector must be taken into consideration. We anticipate that the present study can be applied to motion-induced electromagnetic waves of a mechano-driven media system[28–30] and information transmission technology such as mechanical antennas.

5. Experimental Section

Numerical Modeling of the Contact-Separation (CS) Mode TENG and Lateral-Sliding (LS) Mode TENG: The basic working process of the CS mode TENG and LS mode TENG was computationally carried out by solving the derived equations, with MATLAB (R2021b, Mathworks Inc). The relevant modelling process is presented in Sections S1 and S2 (Supporting

Information). The correctness and effectiveness of this approach were authenticated through two methods: force calculation employing Coulomb's law and Maxwell stress tensor respectively (Section S4, Supporting Information), and contrast validation between finite element simulation and analytical numeration (Section S5, Supporting Information). Note that all the above calculations were based on the following considerations: 1) all the triboelectric charges are uniformly distributed on the contacting surfaces, and these charges are not lost and dissipated during steady state; 2) subsequently a TENG device is neutral at any time, by which it is regarded as a lumped element; 3) all the simulations are performed in the quasi-electromagnetic field, because the TENGs are generally operated under a low working frequency.

Finite Element Analysis of Momentum Current: Detailed simulations of momentum current were performed with finite element method so as to elaborate the change of momentum current and demonstrate the conservation of momentum during the working of TENGs. All simulations were conducted utilizing COMSOL Multiphysics software taking the CS mode TENG as an example (Figure 2a). Under OC conditions, the total charges distributed on the electrodes of the CS mode TENG were set to be 0, accordingly the floating potential of each electrode were different and changed independently. While at SC conditions, the floating potential of electrode needed to be equal with each other. The potential of all boundaries of the air domain were set to 0. The corresponding simulation parameters are listed in Tables S1 and S2 (Supporting Information).

Supporting Information

Supporting Information is available from the Wiley Online Library or from the author.

Acknowledgements

The authors thank Dr. Xiaoxin Pan for helpful discussion. This work was supported by the National Natural Science Foundation of China (Grant Nos. 62001031, 52192610, 51702018, and 51432005), Youth Innovation Promotion Association, CAS, Fundamental Research Funds for the Central Universities (Grant No. E0E48957), and National Key R&D Project from Minister of Science and Technology (Grant No. 2016YFA0202704).

Conflict of Interest

The authors declare no conflict of interest.

Data Availability Statement

The data that support the findings of this study are available from the corresponding author upon reasonable request.

Keywords

maxwell stress tensor, momentum converter, momentum current, momentum transfer, triboelectric nanogenerator

Received: October 10, 2023
Revised: November 21, 2023
Published online:

[1] Z. L. Wang, *Adv. Energy Mater.* **2020**, *10*, 2000137.
[2] Z. L. Wang, *Rep Prog Phys* **2021**, *84*, 096502.
[3] J. Shao, M. Willatzen, Z. L. Wang, *J. Appl. Phys.* **2020**, *128*, 111101.
[4] J. Shao, T. Jiang, Z. Wang, *Sci. Abstr. China, Tech. Sci.* **2020**, *63*, 1087.
[5] S. Niu, Z. L. Wang, *Nano Energy* **2015**, *14*, 161.
[6] K. Dai, X. Wang, S. Niu, F. Yi, Y. Yin, L. Chen, Y. Zhang, Z. You, *Nano Res.* **2016**, *10*, 157.
[7] R. D. I. G. Dharmasena, K. D. G. I. Jayawardena, C. A. Mills, J. H. B. Deane, J. V. Anguita, R. A. Dorey, S. R. P. Silva, *Energy Environ. Sci.* **2017**, *10*, 1801.
[8] R. D. I. G. Dharmasena, K. D. G. I. Jayawardena, C. A. Mills, R. A. Dorey, S. R. P. Silva, *Nano Energy* **2018**, *48*, 391.
[9] J. H. B. Deane, R. D. I. G. Dharmasena, G. Gentile, *Nano Energy* **2018**, *54*, 39 .
[10] J. Shao, M. Willatzen, Y. Shi, Z. L. Wang, *Nano Energy* **2019**, *60*, 630.
[11] J. Shao, D. Liu, M. Willatzen, Z. L. Wang, *Appl. Phys. Rev.* **2020**, *7*, 011405.
[12] X. Guo, J. Shao, M. Willatzen, X. Wang, Z. L. Wang, *Adv. Phys. Res.* **2022**, *2*, 2200039.
[13] X. Guo, J. Shao, M. Willatzen, Y. Yang, Z. L. Wang, *J. Phys. D: Appl. Phys.* **2022**, *55*, 345501.
[14] X. Guo, J. Shao, M. Willatzen, Y. Yang, Z. L. Wang, *Nano Energy* **2022**, *92*, 106762.
[15] C. Fan, J. Shao, X. Guo, M. Willatzen, Z. L. Wang, *Mat. Today Phys.* **2023**, *35*, 101124.
[16] X. Wang, S. Niu, Y. Yin, F. Yi, Z. You, Z. L. Wang, *Adv. Energy Mater.* **2015**, *5*, 1501467.
[17] Z. L. Wang, *Mater. Today* **2017**, *20*, 74.
[18] Z. L. Wang, *Nano Energy* **2020**, *68*, 104272.
[19] J. Shao, M. Willatzen, T. Jiang, W. Tang, X. Chen, J. Wang, Z. L. Wang, *Nano Energy* **2019**, *59*, 380.
[20] S. Niu, Y. S. Zhou, S. Wang, Y. Liu, L. Lin, Y. Bando, Z. L. Wang, *Nano Energy* **2014**, *8*, 150.
[21] J. Peng, S. D. Kang, G. J. Snyder, *Sci. Adv.* **2017**, *3*, eaap8576.
[22] R. D. I. G. Dharmasena, J. H. B. Deane, S. R. P. Silva, *Adv. Energy Mater.* **2018**, *8*, 1802190.
[23] J. Shao, Y. Yang, O. Yang, J. Wang, M. Willatzen, Z. L. Wang, *Adv. Energy Mater.* **2021**, *11*, 2100065.
[24] A. N. May, *Rep Prog Phys* **1936**, *3*, 89.
[25] A. L. Kholmetskii, *Eur J Phys* **2006**, *27*, 825.
[26] M. V. Davidovich, *Phys.-Usp* **2010**, *53*, 595.
[27] D. J. Griffiths, *Introduction to Electrodynamics*, 3rd ed., Prentice-Hall, Hoboken, NJ, USA **2005**, pp. 345–358.
[28] Z. L. Wang, *Mater. Today* **2022**, *52*, 348.
[29] Z. L. Wang, *J Phys Commun* **2022**, *6*, 085013.
[30] Z. L. Wang, *Int J Mod Phys B* **2022**, *37*, 2350159.